# Surface Interactions with Compartmentalized Cellular Phosphates Explain Rare Earth Oxide Nanoparticle Hazard and Provide Opportunities for Safer Design

Ruibin Li,[†] Zhaoxia Ji,[‡] Chong Hyun Chang,[‡] Darren R. Dunphy,[§] Xiaoming Cai,[⊥] Huan Meng,[†] Haiyuan Zhang,[‡] Bingbing Sun,[†] Xiang Wang,[‡] Juyao Dong,[∥] Sijie Lin,[‡] Meiying Wang,[†] Yu-Pei Liao,[†] C. Jeffrey Brinker,[§] Andre Nel,[†,‡,*] and Tian Xia[†,‡,*]

[†]Division of NanoMedicine, Department of Medicine, University of California, 10833 Le Conte Avenue, Los Angeles, California 90095, United States, [‡]California NanoSystems Institute, University of California, 570 Westwood Plaza, Los Angeles, California 90095, United States, [§]Department of Chemical and Nuclear Engineering, University of New Mexico, University of New Mexico MSC01 1120, Albuquerque, New Mexico 87131, United States, [⊥]Department of Pharmacology, School of Medicine, University of California, 360 Med Surge II, Irvine, California 92697, United States, and [∥]Department of Chemistry & Biochemisty, University of California, 607 Charles E. Young Drive East, Los Angeles, California 90095, United States

ABSTRACT Growing international exploitation of rare earth oxides (REOs) for commercial and biological use has increased the possibility of human exposure and adverse health effects. Occupational exposure to rare earth materials in miners and polishers leads to a severe form of pneumoconiosis, while gadolinium-containing MRI contrast agents cause nephrogenic systemic fibrosis in patients with renal impairment. The mechanisms for inducing these adverse pro-fibrogenic effects are of considerable importance for the safety assessment of REO particles as well as presenting opportunities for safer design. In this study, using a well-prepared REO library, we obtained a mechanistic understanding of how REOs induce cellular and pulmonary damage by a compartmentalized intracellular biotransformation process in lysosomes that results in pro-fibrogenic growth factor production and lung fibrosis. We demonstrate that rare earth oxide ion shedding in acidifying macrophage lysosomes leads to biotic phosphate complexation that results in organelle damage due to stripping of phosphates from the surrounding lipid bilayer. This results in nanoparticle biotransformation into urchin shaped structures and setting in motion a series of events that trigger NLRP3 inflammasome activation, IL-1β release, TGF-β1 and PDGF-AA production. However, pretreatment of REO nanoparticles with phosphate in a neutral pH environment prevents biological transformation and pro-fibrogenic effects. This can be used as a safer design principle for producing rare earth nanoparticles for biological use.
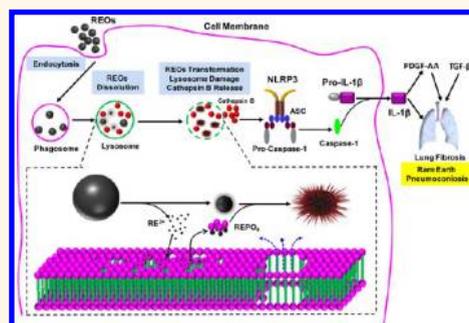
Rare earth oxides (REOs) are increasingly used in products such as magnets, catalysis, electronics, mechanics and fuel additives (*e.g.*, CeO$_2$) because of their unique optical, electronic and magnetic properties.[1,2] Not only has this resulted in increased worker exposure, but there has also been a worldwide increase in rare earth (RE) mining activities as a result of Chinese restrictions on the export of these strategically important materials. Moreover, REOs are also being used incrementally as nanoparticles for biological applications such as biosensors,

luminescence probes and Gadolinium (Gd)-based MRI contrast agents.[3−6] Thus, biological use as well as incidental human exposure has generated the possibility for increased adverse health effects. Not only is there literature showing pneumoconiosis (lung fibrosis) in polishers and RE mining workers,[7] but it is known that administration of Gd-based MRI agents can induce systemic fibrosis in patients with renal impairment, a.k.a., nephrogenic systemic fibrosis (NSF).[8]

In spite of the well-documented adverse health effects induced by RE materials, the

detailed mechanism of how RE materials induce these pathological changes is unclear, especially the structure–activity relationships that explain the mechanism of how the unique physicochemical properties of REOs relate to biological injury responses. REOs are known to be more soluble under acidic conditions[9] and RE ions (III) have high binding affinity to phosphate groups.[10] Recent studies have shown that La_2O_3 and Yb_2O_3 nanoparticles could transform to needle-like $LaPO_4$ nanoclusters in cucumber roots.[11,12] However, it is not clear whether a similar transformation takes place in mammalian tissues, and whether similar processes take place in the lung of workers exposed to REOs. We do know, however, that RE elements that lead to pneumoconiosis are taken up into the lysosomal compartment of macrophages.[13] Macrophage uptake of Gd can also be observed at the systemic sites of collagen deposition in patients with MRI contrast agent induced NSF.[14] Interestingly, Gd-based compounds have also been shown to induce NLRP3 dependent IL-1β production,[14] fibrocyte differentiation and collagen production in a NSF setting.[15−17] In addition, it is also shown that the NLRP3 inflammasome is a major cellular source for IL-1β production and contributes to pulmonary fibrosis.[18,19] While a number of studies have shown that long aspect ratio (LAR) nanomaterials such as CeO_2 nanorods,[20] carbon nanotubes[21] and TiO_2 nanobelts[22] can promote pulmonary fibrosis through NLRP3 inflammasome activation, it is not known how REOs trigger this pathway.

On the basis of the above background, we hypothesized that REOs may undergo biological transformation in an acidic lysosomal compartment to initiate a series of biological responses that trigger lung fibrosis. To test this hypothesis, we established a library of 10 commercial REOs, which were studied in phagolysosomal simulated fluid (pH 4.5) as well as in the lysosomal compartment of macrophages. We observed a pH dependent biological transformation process that results in phosphate deposition on the particle surface and stripping of phosphate groups from the lysosomal membrane lipids. This triggers NLRP3 inflammasome activation and sets in motion a series of events that culminate in pulmonary fibrosis in mice. We also demonstrated that incubation of REO nanoparticles with phosphates in a neutral pH environment passivates the particle surface, thereby preventing lysosomal damage and pulmonary fibrosis.

RESULTS AND DISCUSSION

Abiotic Transformation of REO Nanoparticles in Phagolysosomal Simulated Fluid (PSF). Among the 17 RE elements in the periodic table, 10 commercially available REO nanoparticles (Y_2O_3, La_2O_3, CeO_2, Nd_2O_3, Sm_2O_3, Eu_2O_3, Gd_2O_3, Dy_2O_3, Er_2O_3, and Yb_2O_3) were selected for extensive physicochemical characterization. Most nanoparticles had primary sizes of 18−60 nm, except for Nd_2O_3, Sm_2O_3 and Er_2O_3, which ranged from 100 to 140 nm. In aqueous media, most nanoparticles formed aggregates with hydrodynamic diameters of 300−800 nm, except Y_2O_3, which formed particles of 1346 nm in water (Table S1). In addition, the majority of REOs had isoelectric points of 6.4−8.4, with the zeta potentials ranging from −20 to 20 mV at pH 7.4. In contrast, La_2O_3 and Y_2O_3 exhibited isoelectric points of 9.4 and 9.6 with zeta potentials of 54.3 and 42.7 mV, respectively (Table S2). Because REOs are known to be more soluble under acidic conditions,[9] and are taken up into macrophage lysosomes in the lungs of exposed workers,[13] we compared the behavior of the nanoparticles in PSF *versus* their behavior in water. Interestingly, all REO nanoparticles, except for CeO_2, underwent a significant morphological transformation in PSF as determined by transmission electron microscopy (TEM) (Figure 1A and S1A) and elemental analysis (Figure 1C). Noteworthy, the transformation of the light lanthanide nanoparticles (La_2O_3, Nd_2O_3, Sm_2O_3, Eu_2O_3, and Gd_2O_3) led to the formation of "sea urchin" shaped structures, which displayed needle-like protrusions (Figure 1A), while PSF exposure of the heavy lanthanide NPs (Dy_2O_3, Er_2O_3, and Yb_2O_3), along with Y_2O_3, resulted in structures composed of a network of disordered mesh-like nanowires (Figure S1A). Such morphological changes were not seen for control nanoparticles (Bi_2O_3 and TiO_2) exposed to PSF (Figures 1A and S1A).

To understand in more detail the nature of the REO transformation process in PSF, time-dependent X-ray powder diffraction (XRD) and TEM analyses were performed on La_2O_3 nanoparticles exposed to PSF (Figure 1B). XRD analysis showed lanthanum hydroxide ($La(OH)_3$) and lanthanum oxide carbonate ($La_2O_2-CO_3$) to be the principle phases of the purchased material, which is consistent with observations that RE sesquioxides readily react with ambient water and/or carbon dioxide to form hydroxides and carbonates.[23] However, when placed in PSF, a dynamic transformation takes place during which new $LaPO_4$ peaks can be seen within 15 min, culminating in complete transformation within ∼24 h (Figure 1B). To determine whether $La(OH)_3$ and $La_2O_3-CO_3$ contributed to this transformation, we performed calcination at 825 °C to obtain pure La_2O_3, prior to PSF exposure, and found a similar transformation as for $La_2O_2-CO_3$ and $La(OH)_3$ (Figure S1B). This shows that the impurities have an insignificant effect on the outcome. TEM analysis identified three stages of the transformation process: whisker formation, whisker growth, and ultimately transformation to urchin-shaped structures. XRD peak positions (Figure 1B) match well to the hexagonal rhabdophane polymorph of lanthanide orthophosphate with space group symmetry $P6222$ (PDF#00-046-1439).[24]
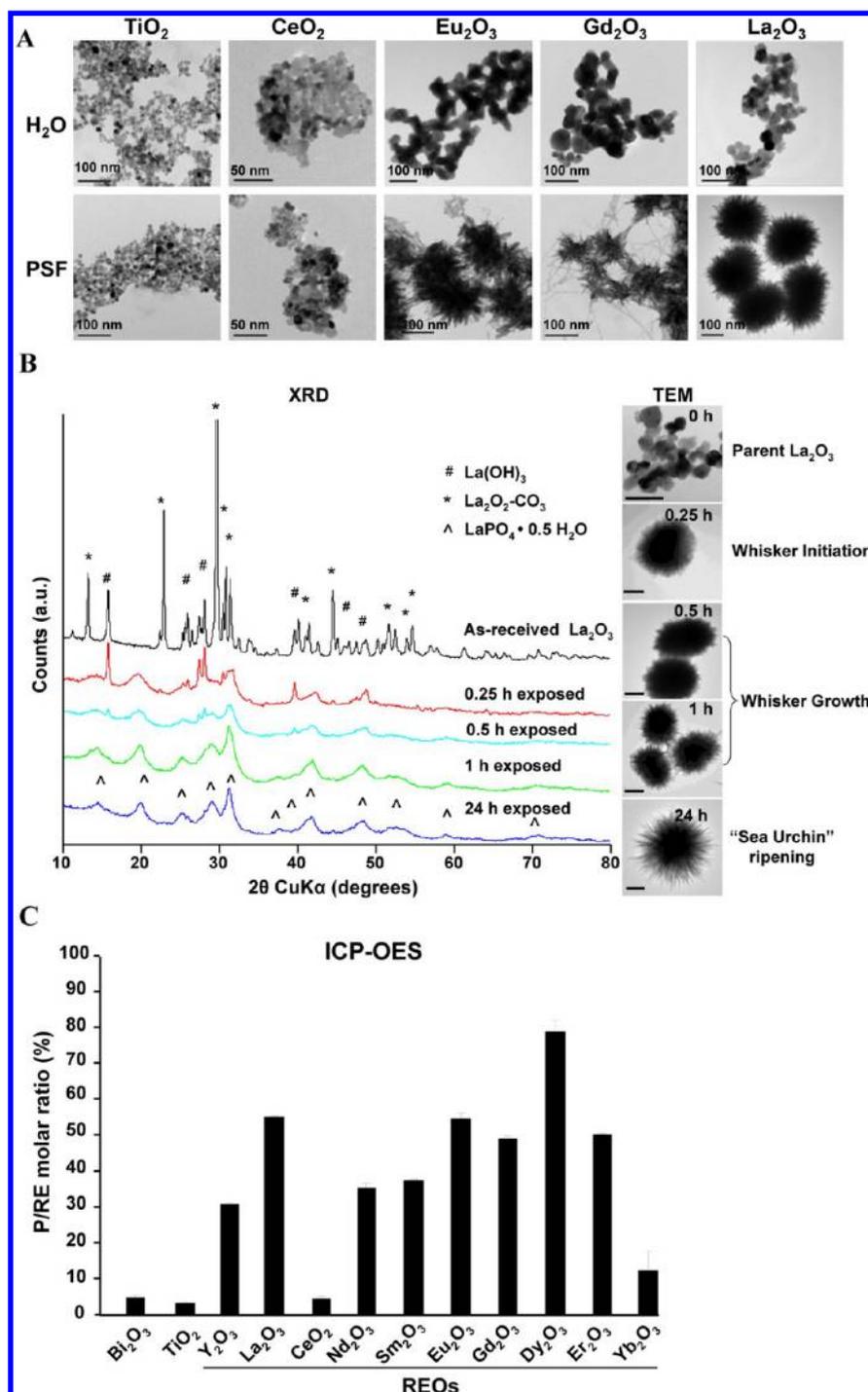
Figure 1. Morphological change and transformation of REOs in PSF. (A) Morphological analysis of REOs after PSF exposure. Nanoparticles were suspended in H_2O or PSF at 50 μg/mL and incubated at 37 °C for 24 h. After washing in H_2O, the morphological changes in the REO nanoparticles were observed under TEM. **(B)** Dynamic monitoring of the transformation process of La_2O_3 nanoparticles suspended in PSF at 50 μg/mL for 0, 0.25, 0.5, 1, or 24 h, before washing and analysis by XRD or TEM (scale bar, 100 nm). **(C)** Molar ratios of phosphorus and metal elements determined by ICP-OES for nanoparticles treated in PSF for 24 h.

To date, lanthanide orthophosphates with nanowire-like structures have been synthesized almost exclusively by hydrothermal methods.[25,26] The low temperature transformation process we report here relies on the greatly enhanced solubility of REOs (oxides, hydroxides, and carbonates) under acidic

biological conditions as well as the extreme insolubility of lanthanide phosphates compared to oxides (K_D = -25 to -27)[10] (Figure S1C). This suggests that the transformation is dependent on rapid La_2O_3 dissolution, leading to the release of La^{3+} and subsequent complexation with PO_4^{3-}. This was confirmed by similar

transformations observed in a simple sodium phosphate buffer at pH 4.5 (Figure S1B). Unlike hydrothermal studies to date,[25] transformation of light lanthanides resulted in sea urchin-like nanostructures with high aspect nanowires emanating from a spherical core (Figure 1A) as opposed to nanowires, and transformation of heavy lanthanide oxides and yttrium oxide resulted in weakly crystalline nanowire meshes (with P/RE ratios ranging from ∼10−80%, Figure S1A,C) as compared to tetragonal nanoparticles.[25] To date, similar morphological changes have only been shown for limited REO nanoparticles including La_2O_3 and Yb_2O_3 in cucumbers.[11,12] Unlike other REO nanoparticles, CeO_2 remains substantially nontransformed (Figure 1A). The reason is that CeO_2 exhibits a higher K_{sp} (10^{-53}) in water than other REOs (K_{sp}, 10^{-21}),[27] and is highly insoluble at both pH 7 and 4.5 (Figure S1C). This further supports our proposed mechanism of the transformation process.

Biotic Transformation of REOs Leading to NLRP3 Inflammasome Activation in Macrophages. Because respirable RE dust can lead to chronic lung disease through targeting of macrophages, we investigated whether engineered REO nanoparticles would undergo biotransformation in THP-1 cells, a myeloid cell line that is often used as an *in vitro* model for studying the effects of engineered nanoparticles on phagocytic cells.[13,28] In particular, THP-1 cells have been proven helpful to study the pro-inflammatory and pro-fibrotic effects of LAR nanomaterials such as multiwalled carbon nanotubes (MWCNTs).[21,29] Using confocal microscopy to study uptake of fluorescein isothiocyanate (FITC)-labeled La_2O_3 and Gd_2O_3 nanoparticles, we found that most of the labeled nanoparticles colocalized with an Alexa fluor 594-labeled LAMP1-positive compartment with coefficients of colocalization ranging from 66 to 91% by Image J analysis (Figure 2A and S2A). This shows that REO nanoparticles localize in lysosomes of THP-1 cells. TEM data confirmed La_2O_3 transformation into urchin-shaped structures in a vesicular THP-1 compartment (Figure 2A). Energy dispersive X-ray (EDX) analysis confirmed the presence of phosphorus peaks in these phagocytized La_2O_3 nanoparticles, suggesting that a particle taken up into an acidifying intracellular compartment undergoes dissolution and phosphate complexation. Gd_2O_3, Eu_2O_3, Sm_2O_3 and Nd_2O_3 nanoparticles also exhibited similar surface changes after cellular uptake in THP-1 cells, while the control TiO_2 nanoparticles did not reveal similar changes (Figure S2B).

To understand the biological impact of REO transformation in the lysosomal compartment, we asked whether there is any effect on lysosomal function, which represents a target for LAR injury in the lung.[20] Confocal microscopy was used to study the subcellular localization of cathepsin B, a lysosomal enzyme capable of cleaving a Magic Red-labeled substrate.[21] As shown in Figure 2B, untreated cells showed a punctate distribution of Magic Red, indicating that the enzyme is contained in intact lysosomes. However, after lysosomal damage by monosodium urate (MSU) (used as a positive control), there was a diffuse cytosolic release of the fluorescence marker.[21] Similarly, Dy_2O_3, Gd_2O_3, La_2O_3, and Nd_2O_3 nanoparticles induced cathepsin B release, while CeO_2 and TiO_2 nanoparticles were not associated with lysosomal damage (Figure 2B). Since cathepsin B is known to contribute to the activation of the NLRP3 inflammasome and IL-1β production,[30,31] which is implicated in chronic lung inflammation and fibrosis by MWCNTs,[19,32,33] we assessed IL-1β release to the supernatant of REO-exposed THP-1 cells. This showed that all REOs, with the exception of CeO_2 and non-REO nanoparticles (see below), could induce IL-1β release to the cellular supernatant (Figure 2B). This effect was dose-dependent (Figure S3D) and required cellular uptake, as demonstrated by a decrease in IL-1β release in cells treated with the cytoskeletal inhibitor, cytochalasin D (Figure S3E and S3F).[34] The role of cathepsin B in NLRP3 inflammasome activation was confirmed by using a cathepsin B inhibitor, CA-074-Me, to show the inhibitory effect in IL-1β production (Figure S3G). Moreover, we confirmed that active assembly of the NLRP3 inflammasome subunits is required for IL-1β production by using NLRP3- and ASC- gene knockdowns to show the interference in cytokine release in THP-1 cells (Figure S3H).

To demonstrate the specific role of REOs in triggering IL-1β release, we compared the effect of 13 transition metal oxides (TMOx) and five post-transition metal oxides (PTMOx) (Figure 2B). All the nanoparticles were fully characterized for isoelectric point (Table S1), primary and hydrodynamic sizes (Figure S3A, Table S2) as well as endotoxin content (Figure S3B). We also determined their effects on THP-1 cell viability by using the MTS assay (Figure S3C). None of the REOs induced changes in cell viability in spite of the lysosomal damage. As expected, some TMOx nanoparticles (CuO, ZnO, Cr_2O_3, CoO, Co_3O_4, and Ni_2O_3) induced dose-dependent cell death in THP-1 cells, which is consistent with our previous report.[35] Analysis of the cellular supernatants demonstrated that the TMOx or PTMOx particles do not trigger IL-1β release. Those effects involve particle dissolution or redox activity, without any effects on the lysosome or the NRLP3 inflammasome. In addition to effects on IL-1β release, REOs could also initiate PDGF-AA production when a human bronchial epithelial cell line (BEAS-2B) was cocultured with THP-1 cells (Figure S4).[21] This is relevant from the perspective of the pulmonary toxicity of LAR materials (*e.g.*, MWCNTs), where afferent triggering of IL-1β production by macrophages initiates a series of events in which
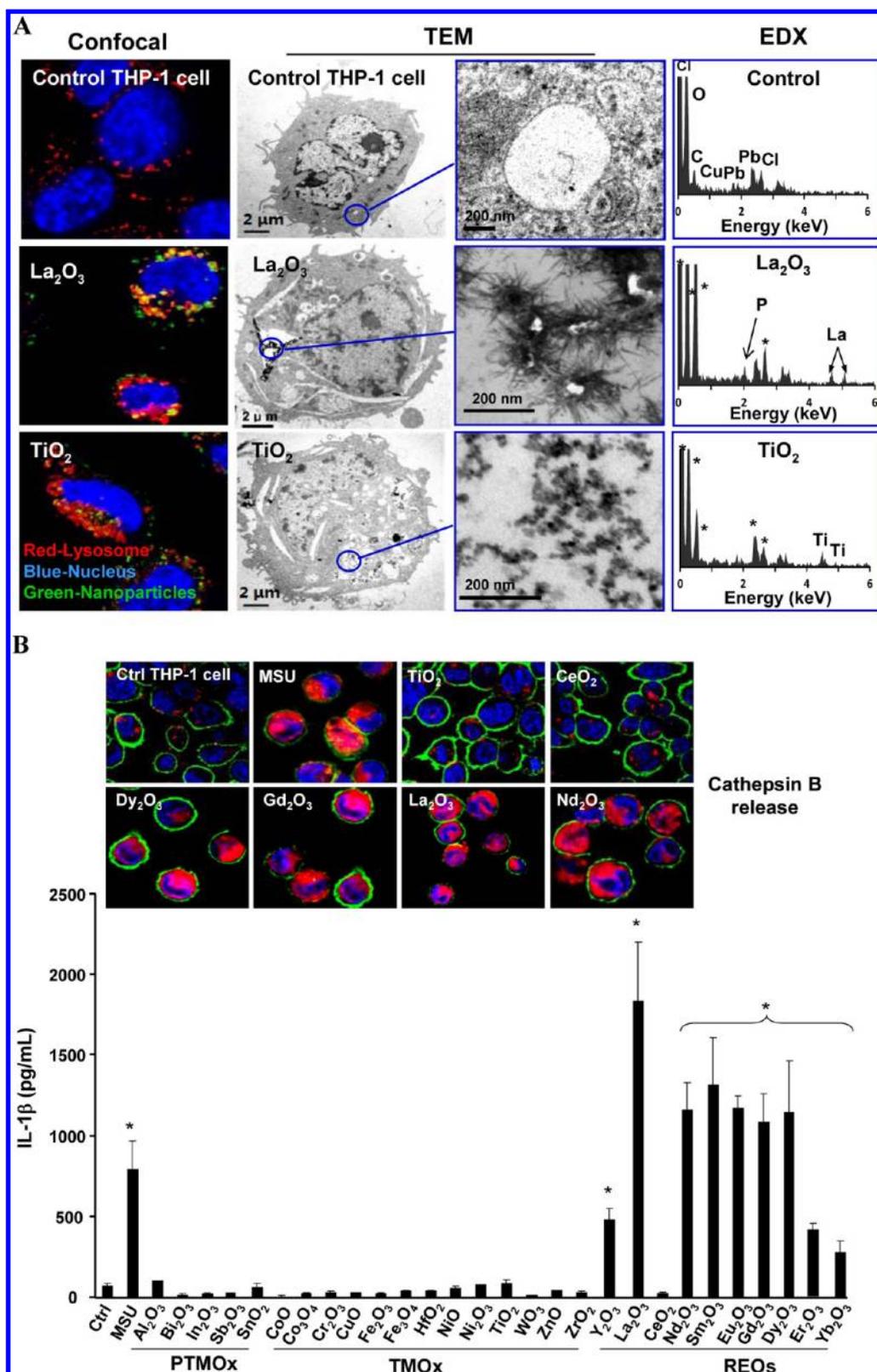
Figure 2. Cellular uptake, biotransformation, and the pro-inflammatory effects of REOs in THP-1 cells. (A) Particle uptake in THP-1 cells was determined by confocal microscopy and TEM. For confocal studies, the cells were incubated with 12.5 μg/mL FITC-labeled particles for 12 h, before washing and staining with Hoechst 33342 dye (blue) and Alexa fluor 594-labeled LAMP1 antibody to identify nuclei and lysosomes, respectively. EDX was used to characterize the cellular particle transformation. An asterisk in the EDX spectra represents background elements. (B) Lysosomal damage, cathepsin B release and IL-1β production after THP-1 cells were treated with 50 μg/mL nanoparticles for 6 h. The cells were stained with Magic Red and visualized by confocal microscopy. IL-1β production was assessed 24 h after treatment with 50 μg/mL nanoparticles. *$p < 0.05$ compared to untreated THP-1 cells.

downstream PDGF-AA (and TGF-β1) production plays a role as pro-fibrogenic factors leading to lung fibrosis.[32]

Lipid Membrane Dephosphorylation as the Key Mechanism of REO-Induced Lysosomal Damage. To explore the mechanism of lysosomal damage, we considered the effect of shape, including whether the needles settling on the particle surface could penetrate the organelle membrane (Figure S5). To test this hypothesis, urchin-shaped nanoparticles (prepared in PSF) were used to expose THP-1 cells. However, this did not lead to lysosome damage or IL-1β release in spite of similar levels of cellular uptake (Figure S6). This argues against a shape effect only. We therefore explored a second mechanism involving dephosphorylation of critical phospholipids that play a role in the structural integrity of lysosomes. To test this hypothesis, we used propidium iodide (PI) loaded liposomes (made from phosphatidic acid) to assess PI leakage after incubation with selected REO nanoparticles. La$_2$O$_3$ and Gd$_2$O$_3$ induced significantly higher levels of PI leakage ($\sim$ 30−35%) compared to control particles (CeO$_2$, Bi$_2$O$_3$ and TiO$_2$) (<8%) (Figure 3A). We also assessed the phosphate content of the lysosome remnants, using liquid chromatography coupled to mass spectrometry (LC−MS) (Figure 3A). This demonstrated that La$_2$O$_3$ and Gd$_2$O$_3$ could induce the dephosphorylation of 2.5% and 1.6% of the phosphatidic acid content, respectively (right-hand panel). These results are in favor of phospholipid dephosphorylation as the principal injury mechanism. In contrast, CeO$_2$ induced minimal (0.2%) dephosphorylation while TiO$_2$ or Bi$_2$O$_3$ had no effect on the phosphate content of phospholipids. The ability to damage membranes was also confirmed by studying red blood cells (RBCs). Performance of hemolysis assays[36] in the absence or presence of phosphate demonstrated little or no RBC lysis in the presence of 10 mM phosphate, while all the REOs (except CeO$_2$) could lyse up to 22% of the RBCs in the absence of phosphate (Figure 3B). This hemolytic effect is dose dependent (Figure S7). TiO$_2$ and Bi$_2$O$_3$ did not exert similar effects. These data suggest that REOs damage the lysosomal membrane by stripping the membrane phosphate groups.

***In Vivo* Transformation of REOs Leads to Pulmonary Fibrosis in Mice.** To explore the impact of La$_2$O$_3$ nanoparticles on pulmonary alveolar macrophages *in vivo*, we used oropharyngeal nanoparticle aspiration, followed by the recovery of primary alveolar macrophages from the bronchoalveolar lavage fluid (BALF) 40 h later. TEM analysis demonstrated particle uptake in membrane-lined vacuoles, which, upon EDX analysis, showed the presence of LaPO$_4$ in needle-shaped particles (Figure 4A). In contrast, there was no significant morphological change in TiO$_2$ nanoparticles, which do not biotransform in the presence of phosphate. We also

demonstrated that while REOs induce lysosomal damage and cathepsin B release in alveolar macrophages, TiO$_2$ nanoparticles did not exert a similar effect (Figure 4B). These results show that phosphate-mediated biotransformation is responsible for lysosomal damage in alveolar macrophages in the intact lung.

In a subsequent experiment looking at the effect on the whole lung, we used a subchronic lung injury model to study the effect of oropharyngeal instilled nanoparticles on fibrosis. These studies were performed with a particle dose of 2 mg/kg, which has previously been determined to fall on the linear part of the dose−response curve for pulmonary exposure to metal oxide nanoparticles.[21,29] Considering the real life exposure scenarios in the workplace,[37,38] the airborne level of nanoparticles could be $\sim$300−1100 μg/m^3. A worker, exposed to 400 μg/m^3 nanoparticles for 8 h/day over a five-month time period for a working lifetime, could exhibit a lung burden similar to 2 mg/kg bolus exposure in the mouse.[21]

Mice exposed to Gd$_2$O$_3$, La$_2$O$_3$, Er$_2$O$_3$, Yb$_2$O$_3$ and TiO$_2$ nanoparticles were sacrificed after 21 days to examine the BALF and collect lung tissue. While there was a significant increase in macrophage numbers in the BALF of animals treated with REO nanoparticles, neutrophil counts remained at background levels (Figure S8A). Hematoxylin and eosin (H&E) staining also did not show significant histological changes (Figure S8B). However, the BALF from animals exposed to REO nanoparticles showed significant increases in IL-1β, TGF-β1 and PDGF-AA levels (Figure 4C). Moreover, the Sircol assay showed that the presence of these pro-fibrogenic factors is accompanied by increased total lung collagen content, which was further confirmed by collagen deposition around small airways in Trichrome stained lung sections (Figure 4D). Similar effects were not observed in animals exposed to TiO$_2$ nanoparticles. Taken together, these results show that intrapulmonary transformation of REOs, similar to *in vitro* responses, is associated with adverse biological effects that culminate in pulmonary fibrosis. These experimental findings are in agreement with the pathological findings in rare earth pneumoconiosis.[39−41]

Phosphate Coating at Neutral pH as a Safer Design for REO Particles. Since the particle dissolution and high binding affinity of RE ions (III) to bystander phosphate groups appear to be critical for the hazard-associated biotransformation, we asked whether prior complexation of REO nanoparticles with phosphate under neutral or physiological pH conditions will slow down or eliminate the material bioreactivity that leads to *in vitro* and *in vivo* toxicity. As-received La$_2$O$_3$ nanoparticles were suspended at 50 μg/mL in a 10 mM phosphate buffer solution (pH 7.4) at 37 °C for 24 h. Figure 5A shows that prior phosphate complexing at pH 7.4 did

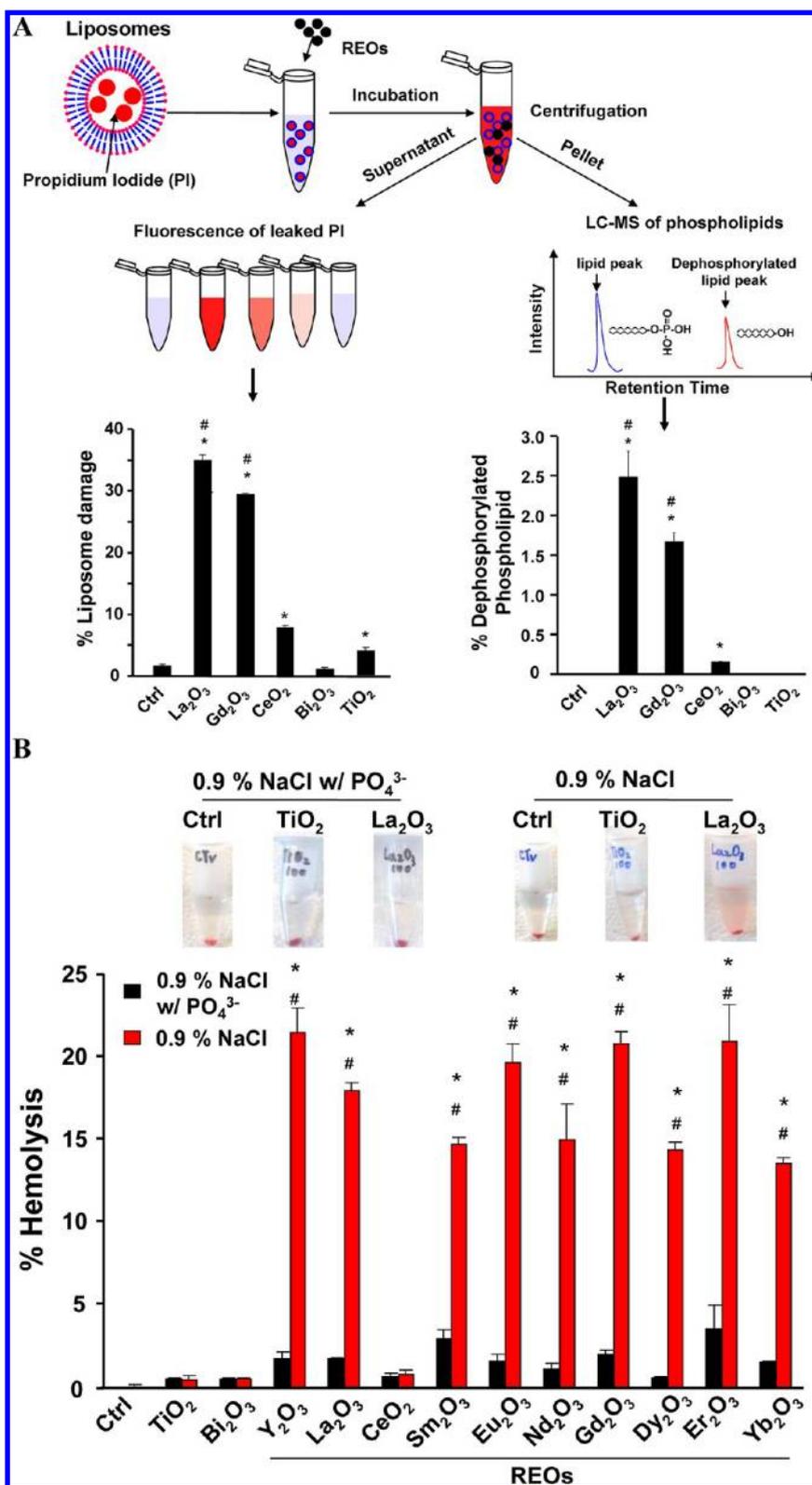**Figure 3. REOs induce membrane damage through phospholipid dephosphorylation. (A) Liposome damage induced by REOs. A total of 100 μg/mL nanoparticles was incubated with 1 mg/mL propidium iodide (PI) loaded liposomes in saline buffer (pH 7.0) at 37 °C for 3 h. After centrifugation, PI fluorescence in the supernatant was measured. The pelleted phospholipids were used for phosphate analysis by LC−MS. (B) Hemolysis induced by REOs. Freshly prepared mouse red blood cells were incubated with 100 μg/mL nanoparticles in saline with or without phosphate at 37 °C for 3 h, followed by centrifugation at 2000 rpm for 5 min. The supernatants were collected and hemoglobin content was determined by measuring absorbance at 540 nm using a UV−vis spectrometer. *$p < 0.05$ compared to control or samples in saline without phosphate; #$p < 0.05$ compared to CeO_2, TiO_2 and Bi_2O_3.**

not significantly change particle morphology (TEM). Moreover, XRD analysis also did not show a change in the crystallinity. When exposed to PSF, the phosphate-coated La_2O_3 ($PO_4-La_2O_3$) did not transform into urchin-shaped structures and preserved a La_2O_3 crystal structure. Moreover, PO_4-REO and REO nanoparticles showed similar cellular uptake by ICP-OES analysis, suggesting phosphate coating did not affect cellular internalization (Figure S9). However, prior phosphate coating effectively interfered in the hemo-
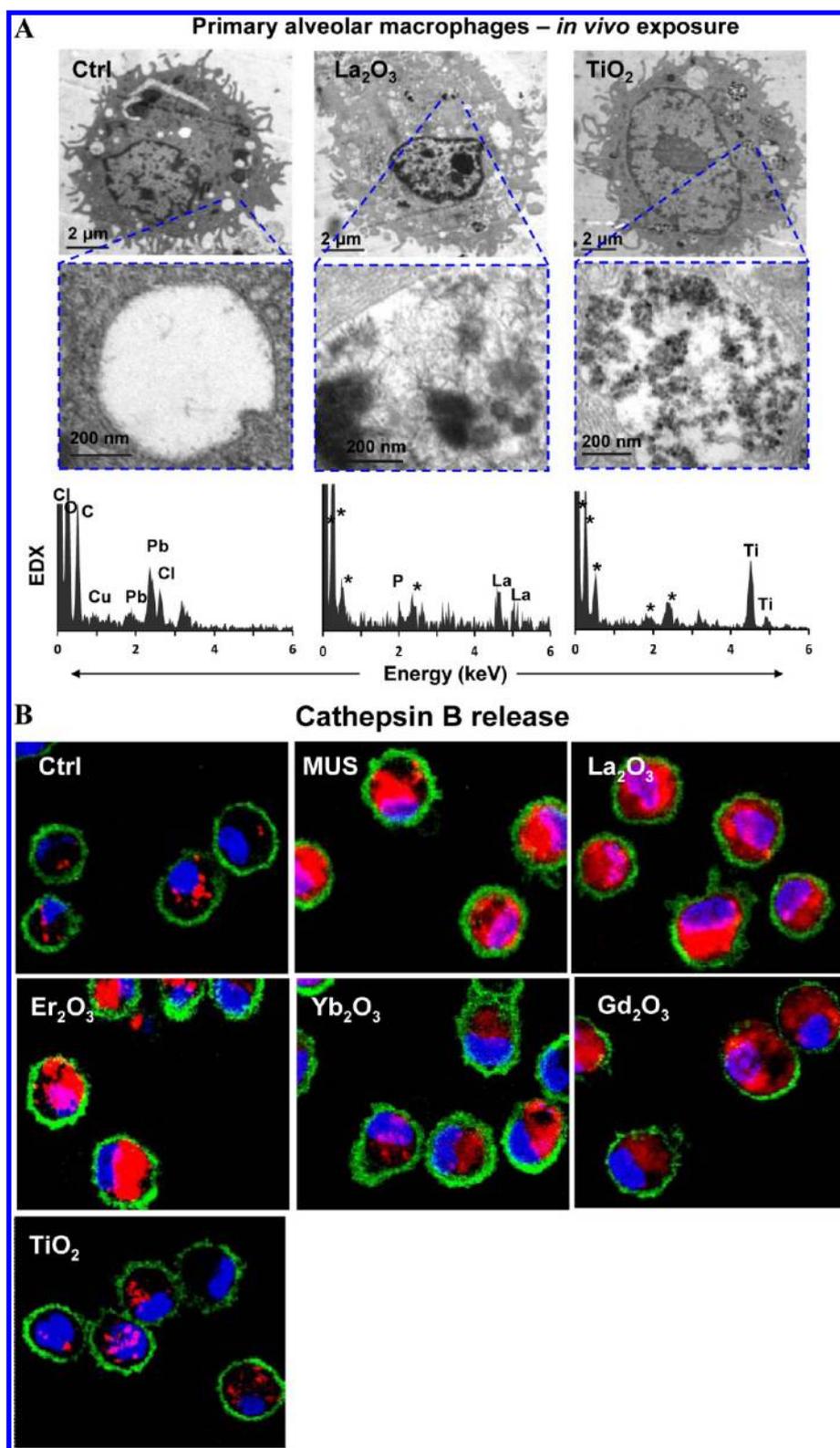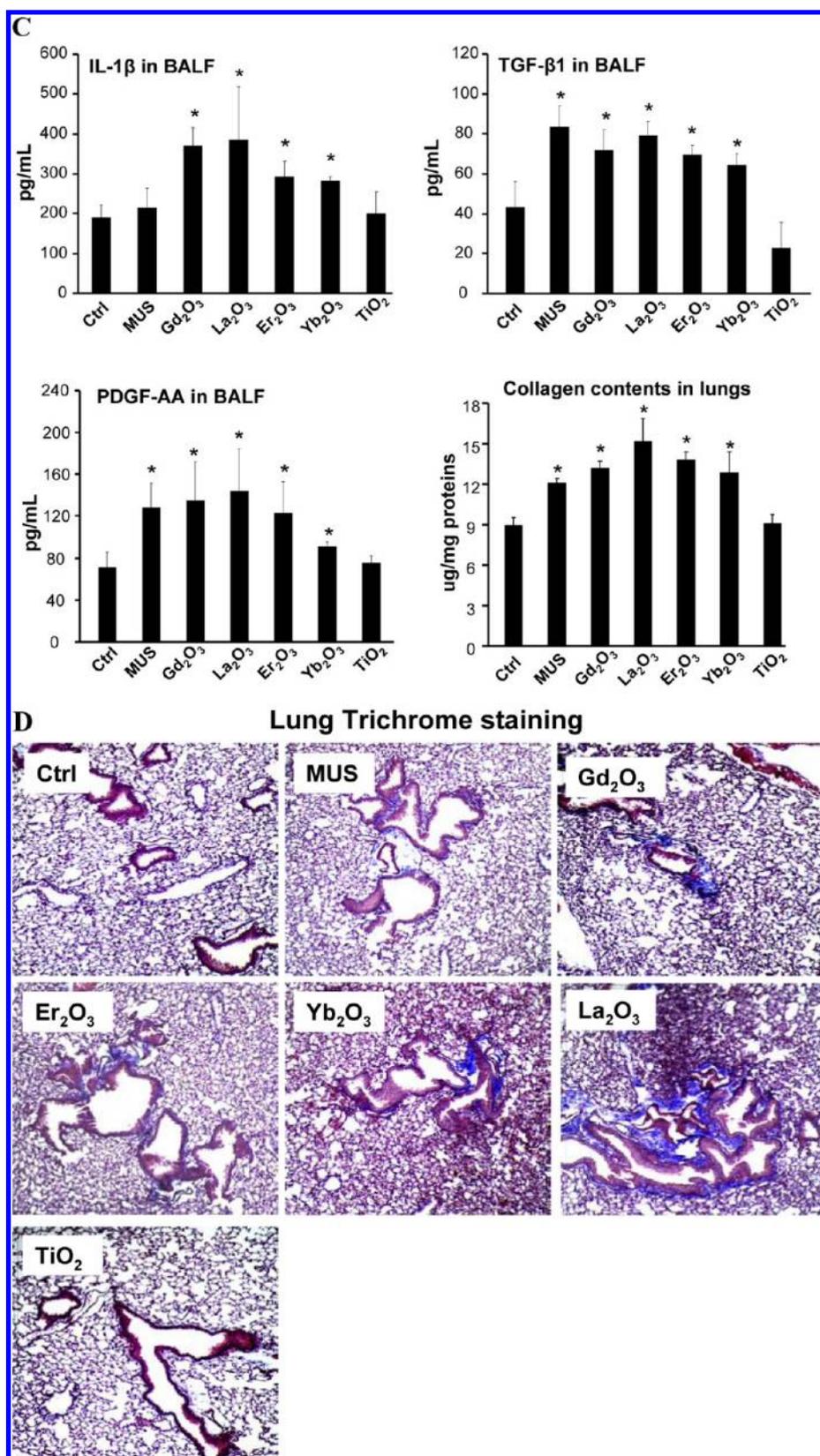
Figure 4. Cellular uptake and biotransformation of REOs in primary alveolar macrophages as well as pulmonary inflammation and fibrosis induced by REOs in mouse lungs. (A) Cellular uptake and biotransformation of REO nanoparticles in primary alveolar macrophages lavaged from the mouse lung after exposure of La_2O_3 or TiO_2 at 2 mg/kg for 40 h (asterisk (*) denotes background elements in the EDX spectra). (B) Lysosomal damage and cathepsin B release in primary alveolar macrophages induced by nanoparticles. The cell staining procedure is similar to Figure 2B. (C) Pro-fibrogenic cytokine production in bronchoalveolar lavage fluid (BALF) and quantification of total collagen deposition in the lung from mice exposed to the nanoparticles at 2 mg/kg for 21 days. (D) Trichrome staining of lung tissues to show the extent of lung fibrosis. *$p < 0.05$ compared to untreated animals.
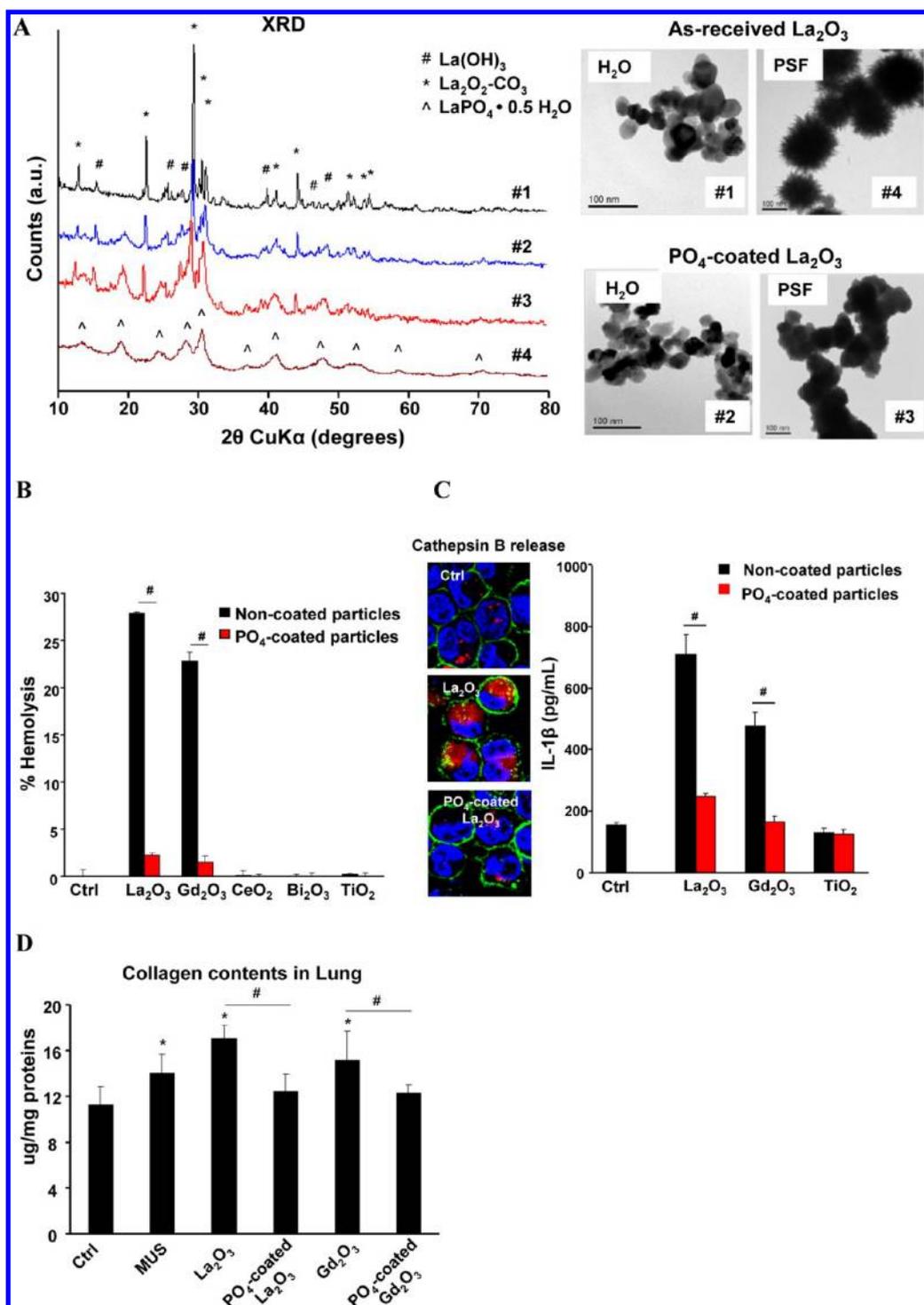
Figure 5. Prevention of REO toxicological effects by prior complexation to phosphate at pH 7.4. (A) Morphological and crystallinity changes of La$_2$O$_3$ nanoparticles in water and PSF with or without prior phosphate coating. Phosphate coated-REOs were prepared by treating 50 μg/mL REO nanoparticles in 10 mM phosphate buffer (pH 7.4) at 37 °C for 24 h. (B) Comparison of the % hemolysis induced by as-received and PO$_4$-coated La$_2$O$_3$ nanoparticles. Freshly prepared mouse red blood cell suspensions were incubated with 100 μg/mL REOs with or without phosphate coating at 37 °C for 3 h. The hemolysis was determined as described in Figure 3B. (C) Cathepsin B release and IL-1β production in THP-1 cells after exposure to 50 μg/mL REOs or PO$_4$-coated REOs at 37 °C for 6 h. (D) Comparison of collagen content in animal lung exposed to coated and uncoated nanoparticles. *p < 0.05 compared to untreated THP-1 cells; #p < 0.05 compared to uncoated REOs.

lytic potential of La$_2$O$_3$ and Gd$_2$O$_3$ nanoparticles (Figure 5B). The phosphate-coated particles also induced significantly less IL-1β release in THP-1 cells (Figure 5C) and prevented collagen deposition in the lung after three weeks (Figure 5D). Moreover, the production of the pro-fibrogenic growth factors, TGF-β1
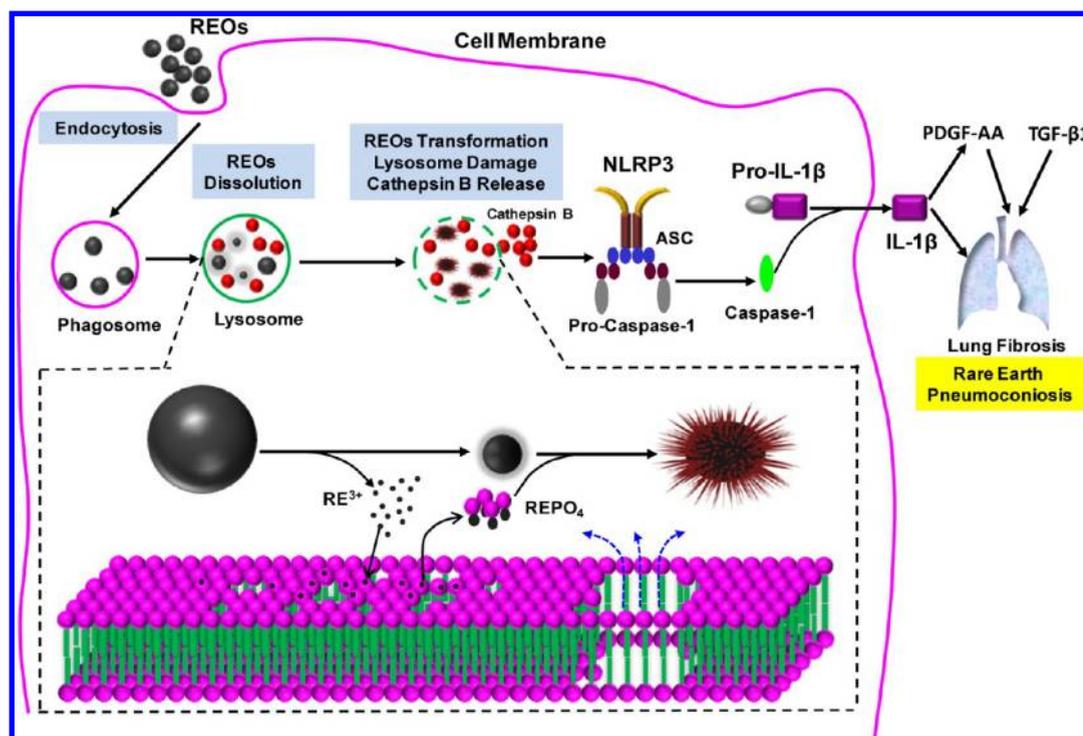
Figure 6. Schematic to explain the cellular mechanisms leading to the pro-fibrogenic effects of REOs. Following the internalization of REOs by macrophages and lysosomal biotransformation, damage to the organelle leads to IL-1β production and triggering of events culminating in pulmonary fibrosis. The inserted panel at the bottom shows that the molecular mechanism of lysosomal damage is phospholipid dephosphorylation and nucleation of REPO$_4$ on the nanoparticle surface. The particles are morphologically transformed to sea urchin structure in the process.

and PDGF-AA, were significantly decreased in the BALF of mice receiving precoated particles (Figure S10).

SUMMARY AND CONCLUSION

All considered, we have elucidated a unique mechanism of REO hazard generation in cells and animals, which is of direct relevance to humans (Figure 6). Macrophage uptake and lysosomal processing of REO nanoparticles lead to enhanced, pH-dependent particle dissolution. The released RE ions (III) are rapidly bound by bystander phosphates resulting in the crystallization of REPO$_4$ deposits on the particle surfaces. This leads to morphological transformation to urchin-shaped or mesh-like structures depending on the REO species. Once the free lysosomal phosphates are depleted, the released RE ions are capable of stripping lysosomal membrane phosphate groups, leading

to organelle damage, cathepsin B release, NLRP3 inflammasome activation and IL-1β release from the macrophages. IL-1β participates in a progressive march of events that include the production of pro-fibrogenic growth factors by epithelial cells, ultimately culminating in pulmonary fibrosis. These findings could explain the development of pneumoconiosis in occupational settings and may also be involved in the pathogenesis of NSF by Gd-containing MRI contrast agents. We demonstrate that prior phosphate coating at a neutral pH constitutes a simple, yet effective way to decrease the hazard potential of REOs. In summary, we have developed a predictive toxicological approach for expedited safety assessment and reducing the toxicity of REO nanoparticles. Improving the safety of REO and upconversion nanoparticles could be of great significance in the development of biological application of these materials.

EXPERIMENTAL SECTION

Transformation of REOs in PSF. Nanoparticles were dissolved in 10 mL PSF buffer (142 mg/L Na$_2$HPO$_4$, 6.65 g/L NaCl, 62 mg/L Na$_2$SO$_4$, 29 mg/L CaCl$_2$·H$_2$O, 250 mg/L glycine, 8.09 g/L potassium phthalate, pH 4.5) at concentration of 50 μg/mL, and sonicated at 32 W for 15 s. Following incubation at 37 °C for 24 h, the nanoparticle suspensions were centrifuged at 15 000 rpm for 10 min. The pellets were collected, thoroughly washed with DI H$_2$O and dried at a room temperature for further use. The composition and morphology of PSF-treated nanoparticles

were characterized by ICP-OES (ICPE-9000, SHIMADZU, Japan), XRD (Panalytical X'Pert Pro diffractometer, Cu Kα radiation) and TEM (JEOL 1200 EX, accelerating voltage 80 kV).

NLRP3 Inflammasome Activation and IL-1β Production. IL-1β production was detected in the culture media of THP-1 cells using a human IL-1β ELISA Kit (BD; San Jose, CA, USA). Briefly, aliquots of 5 × 10^4 wild type, NLRP3$^{-/-}$ or ASC$^{-/-}$ THP-1 cells were seeded in 0.1 mL complete medium and primed with 1 μg/mL phorbol 12-myristate acetate (PMA) overnight in 96-well plates (Corning; Corning, NY, USA). Cells were treated with the desired concentration of the particle suspensions made up in complete

RPMI 1640 medium, supplemented with 10% fetal bovine serum and 10 ng/mL lipopolysaccharide (LPS). The suspensions were sonicated with a sonication probe (Sonics & Materials) at 32 W for 15 s before adding to the cells.

Lysosomal Damage and Cathepsin B Release. THP-1 cells treated with 50 μg/mL nanoparticles in c-RPMI 1640 for 6 h or primary alveolar macrophages from the BALF of animals receiving 2 mg/kg nanoparticles for 40 h were washed with PBS, stained with Magic Red (ImmunoChemistry Technologies) for 1 h, and fixed in 4% paraformaldehyde for 20 min. Following another wash in PBS, cell membranes and nuclei were stained with Alexa Fluor 488-conjugated wheat germ agglutinin (WGA) and Hoechst 33342, respectively, at room temperature for 1 h. The cells were visualized under a confocal microscope (Leica Confocal SP2 1P/FCS). High magnification images were obtained under the 63× objective.

Assessment of Liposome Lysis. Propidium iodide (PI) loaded liposomes were synthesized according to a standardized method.[37] The full method of liposome synthesis is provided in Supporting Information (S-1). The prepared PI loaded liposomes were suspended in saline buffer at 1 mg/mL to yield a PI loaded liposome suspension. A volume of 490 μL of this suspension was mixed with 10 μL of nanoparticles (5 mg/mL), DI H$_2$O or Triton X-100 and incubated at 37 °C for 3 h. The mixture was centrifuged at 100 000 rpm for 30 min, and PI fluorescence in the supernatants was monitored in a SpectraMax M5 microplate spectrophotometer at excitation and emission wavelength of 520 and 580 nm, respectively. The % liposome leakage was calculated by dividing the difference between the absorption of each sample and the negative control by the difference in absorption between the positive and negative controls. Pellets remaining after nanoparticle exposure were extracted by adding 250 μL CHCl$_3$ for LC−MS analysis to calculate the % dephosphorylated phosphatidic acid. For more elaboration of LC−MS analytical methods, please also see the Supporting Information (S-2).

Hemolysis Assay. Mouse blood was washed with saline, following which the RBCs were diluted to 1×10^8 cell/mL in saline or saline plus 10 mM phosphate. Subsequently, 490 μL of a diluted RBC suspension was mixed with 10 μL of nanoparticles (5 mg/mL), DI H$_2$O (negative control) or 0.25% Triton X-100 (positive control). The mixtures were gently stirred and incubated for 3 h at 37 °C. The samples were centrifuged, and the absorbance of the supernatants was measured at 541 nm in a SpectraMax M5 microplate spectrophotometer. The percent hemolysis in each sample was calculated as previously described.[36]

Lung Inflammation and Fibrosis in Mice. Mice were exposed to nanoparticle suspensions using oropharyngeal aspiration at 2 mg/kg. A more detailed description is provided in Supporting Information (S-3).

Statistical Methods. Results were statistically analyzed using one-way ANOVA or Student t test. The difference is regarded statistically significant if the p value is less than 0.05. Data are reported as the mean ± standard deviation from at least three separate experiments.

Conflict of Interest: The authors declare no competing financial interest.

Supporting Information Available: Detailed methods, characterization of metal oxide nanoparticles, acute cytoxicity of metal oxides, IL-1β production, transformation of REOs, dissolution by ICP-OES, PDGF-AA production, cellular uptake by ICP-OES, neutrophil count, H&E staining and cytokine production in animal lungs. This material is available free of charge *via* the Internet at http://pubs.acs.org.

REFERENCES AND NOTES

1. Adachi, G.; Imanaka, N. The Binary Rare Earth Oxides. *Chem. Rev.* **1998**, *98*, 1479–1514.
2. Cassee, F. R.; van Balen, E. C.; Singh, C.; Green, D.; Muijser, H.; Weinstein, J.; Dreher, K. Exposure, Health and Ecological Effects Review of Engineered Nanoscale Cerium and Cerium Oxide Associated with Its Use as a Fuel Additive. *Crit. Rev. Toxicol.* **2011**, *41*, 213–229.
3. Ahren, M.; Selegard, L.; Klasson, A.; Soderlind, F.; Abrikossova, N.; Skoglund, C.; Bengtsson, T.; Engstrom, M.; Kall, P. O.; Uvdal, K. Synthesis and Characterization of Pegylated Gd$_2$O$_3$ Nanoparticles for MRI Contrast Enhancement. *Langmuir* **2010**, *26*, 5753–5762.
4. Bouzigues, C.; Gacoin, T.; Alexandrou, A. Biological Applications of Rare-Earth Based Nanoparticles. *ACS Nano* **2011**, *5*, 8488–8505.
5. Hu, C. G.; Liu, H.; Dong, W. T.; Zhang, Y. Y.; Bao, G.; Lao, C. S.; Wang, Z. L. La(OH)$_3$ and La$_2$O$_3$ Nanobelts—Synthesis and Physical Properties. *Adv. Mater.* **2007**, *19*, 470–474.
6. Louis, C.; Bazzi, R.; Marquette, C. A.; Bridot, J. L.; Roux, S.; Ledoux, G.; Mercier, B.; Blum, L.; Perriat, P.; Tillement, O. Nanosized Hybrid Particles with Double Luminescence for Biological Labeling. *Chem. Mater.* **2005**, *17*, 1673–1682.
7. Vocaturo, G.; Colombo, F.; Zanoni, M.; Rodi, F.; Sabbioni, E.; Pietra, R. Human Exposure to Heavy-Metals-Rare-Earth Pneumoconiosis in Occupation Workers. *Chest* **1983**, *83*, 780–783.
8. Marckmann, P.; Skov, L.; Rossen, K.; Dupont, A.; Damholt, M. B.; Heaf, J. G.; Thomsen, H. S. Nephrogenic Systemic Fibrosis: Suspected Causative Role of Gadodiamide Used for Contrast-Enhanced Magnetic Resonance Imaging. *J. Am. Soc. Nephrol.* **2006**, *17*, 2359–2362.
9. Austreng, E.; Storebakken, T.; Thomassen, M. S.; Refstie, S.; Thomassen, Y. Evaluation of Selected Trivalent Metal Oxides as Inert Markers Used to Estimate Apparent Digestibility in Salmonids. *Aquaculture* **2000**, *188*, 65–78.
10. Firsching, F. H.; Brune, S. N. Solubility Products of the Trivalent Rare-Earth Phosphates. *J. Chem. Eng. Data* **1991**, *36*, 93–95.
11. Zhang, P.; Ma, Y. H.; Zhang, Z. Y.; He, X.; Guo, Z.; Tai, R. Z.; Ding, Y. Y.; Zhao, Y. L.; Chai, Z. F. Comparative Toxicity of Nanoparticulate/Bulk Yb$_2$O$_3$ and YbCl$_3$ to Cucumber (*Cucumis sativus*). *Environ. Sci. Technol.* **2012**, *46*, 1834–1841.
12. Ma, Y.; He, X.; Zhang, P.; Zhang, Z.; Guo, Z.; Tai, R.; Xu, Z.; Zhang, L.; Ding, Y.; Zhao, Y.; *et al.* Phytotoxicity and Biotransformation of La$_2$O$_3$ Nanoparticles in a Terrestrial Plant Cucumber (*Cucumis sativus*). *Nanotoxicology* **2011**, *5*, 743–753.
13. Hirano, S.; Suzuki, K. T. Exposure, Metabolism, and Toxicity of Rare Earths and Related Compounds. *Environ. Health Perspect.* **1996**, *104*, 85–95.
14. Kay, J.; Bossaller, L.; Schmidt-Lauber, C.; Abujudeh, H. H.; Vladimer, G.; Latz, E.; Fitzgerald, K. A.; Marshak-Rothstein, A.; Gravallese, E. M. Gadolinium-Based Compounds Induce NLRP3-Dependent IL-1beta Production and Peritoneal Inflammation. *Arthritis Rheum.* **2013**, *65*, S1246–S1246.
15. Wermuth, P. J.; Jimenez, S. A. Gadolinium Compounds Signaling through Tlr 4 and Tlr 7 in Normal Human Macrophages: Establishment of a Proinflammatory Phenotype and Implications for the Pathogenesis of Nephrogenic Systemic Fibrosis. *J. Immunol.* **2012**, *189*, 318–327.
16. Vakil, V.; Sung, J. J.; Piecychna, M.; Crawford, J. R.; Kuo, P.; Abu-Alfa, A. K.; Cowper, S. E.; Bucala, R.; Gomer, R. H. Gadolinium-Containing Magnetic Resonance Image Contrast Agent Promotes Fibrocyte Differentiation. *J. Magn. Reson. Imaging* **2009**, *30*, 1284–1288.
17. Bucala, R. Circulating Fibrocytes: Cellular Basis for Nsf. *J. Am. Coll. Radiol.* **2008**, *5*, 36–9.
18. Cassel, S. L.; Eisenbarth, S. C.; Iyer, S. S.; Sadler, J. J.; Colegio, O. R.; Tephly, L. A.; Carter, A. B.; Rothman, P. B.; Flavell, R. A.;

Sutterwala, F. S. The Nalp3 Inflammasome Is Essential for the Development of Silicosis. *Proc. Natl. Acad. Sci. U. S. A.* **2008**, *105*, 9035–9040.

19. Artlett, C. M. The Role of the NLRP3 Inflammasome in Fibrosis. *Open Rheumatol. J.* **2012**, *6*, 80–6.

20. Ji, Z.; Wang, X.; Zhang, H.; Lin, S.; Meng, H.; Sun, B.; George, S.; Xia, T.; Nel, A. E.; Zink, J. I. Designed Synthesis of CeO_2 Nanorods and Nanowires for Studying Toxicological Effects of High Aspect Ratio Nanomaterials. *ACS Nano* **2012**, *6*, 5366–5380.

21. Li, R.; Wang, X.; Ji, Z.; Sun, B.; Zhang, H.; Chang, C. H.; Lin, S.; Meng, H.; Liao, Y. P.; Wang, M.; *et al.* Surface Charge and Cellular Processing of Covalently Functionalized Multiwall Carbon Nanotubes Determine Pulmonary Toxicity. *ACS Nano* **2013**, *7*, 2352–2368.

22. Hamilton, R. F.; Wu, N. Q.; Porter, D.; Buford, M.; Wolfarth, M.; Holian, A. Particle Length-Dependent Titanium Dioxide Nanomaterials Toxicity and Bioactivity. *Part. Fibre Toxicol.* **2009**, *6*, 11.

23. Bernal, S.; Botana, F. J.; Garcia, R.; Rodriguezizquierdo, J. M. Behavior of Rare-Earth Sesquioxides Exposed to Atmospheric Carbon-Dioxide and Water. *React. Solids* **1987**, *4*, 23–40.

24. Romero, B.; Bruque, S.; Aranda, M. A. G.; Iglesias, J. E. Syntheses, Crystal-Structures, and Characterization of Bismuth Phosphates. *Inorg. Chem.* **1994**, *33*, 1869–1874.

25. Fang, Y. P.; Xu, A. W.; Song, R. Q.; Zhang, H. X.; You, L. P.; Yu, J. C.; Liu, H. Q. Systematic Synthesis and Characterization of Single-Crystal Lanthanide Orthophosphate Nanowires. *J. Am. Chem. Soc.* **2003**, *125*, 16025–16034.

26. Lai, H.; Bao, A.; Yang, Y. M.; Tao, Y. C.; Yang, H. Selective Synthesis and Luminescence Property of Monazite- and Hexagonal-Type $LaPO_4$: Eu Nanocrystals. *CrystEngComm* **2009**, *11*, 1109–1113.

27. Abreu, R. D.; Morais, C. A. Purification of Rare Earth Elements from Monazite Sulphuric Acid Leach Liquor and the Production of High-Purity Ceric Oxide. *Miner. Eng.* **2010**, *23*, 536–540.

28. Ulker, O. C.; Yucesoy, B.; Demir, O.; Tekin, I. O.; Karakaya, A. Serum and Bal Cytokine and Antioxidant Enzyme Levels at Different Stages of Pneumoconiosis in Coal Workers. *Hum. Exp. Toxicol.* **2008**, *27*, 871–877.

29. Wang, X.; Xia, T.; Duch, M. C.; Ji, Z. X.; Zhang, H. Y.; Li, R. B.; Sun, B. B.; Lin, S. J.; Meng, H.; Liao, Y. P.; *et al.* Pluronic F108 Coating Decreases the Lung Fibrosis Potential of Multiwall Carbon Nanotubes by Reducing Lysosomal Injury. *Nano Lett.* **2012**, *12*, 3050–3061.

30. Duewell, P.; Kono, H.; Rayner, K. J.; Sirois, C. M.; Vladimer, G.; Bauernfeind, F. G.; Abela, G. S.; Franchi, L.; Nunez, G.; Schnurr, M.; *et al.* Nlrp3 Inflammasomes Are Required for Atherogenesis and Activated by Cholesterol Crystals. *Nature* **2010**, *464*, 1357–1361.

31. Duncan, J. A.; Gao, X.; Huang, M. T. H.; O'Connor, B. P.; Thomas, C. E.; Willingham, S. B.; Bergstralh, D. T.; Jarvis, G. A.; Sparling, P. F.; Ting, J. P. Y. Neisseria Gonorrhoeae Cctivates the Proteinase Cathepsin B to Mediate the Signaling Activities of the NLRP3 and Asc-Containing Inflammasome. *J. Immunol.* **2009**, *182*, 6460–6469.

32. Bonner, J. C. Mesenchymal Cell Survival in Airway and Interstitial Pulmonary Fibrosis. *Fibrog. Tissue Repair* **2010**, *3*, 15.

33. Feyerabend, F.; Fischer, J.; Holtz, J.; Witte, F.; Willumeit, R.; Drucker, H.; Vogt, C.; Hort, N. Evaluation of Short-Term Effects of Rare Earth and Other Elements Used in Magnesium Alloys on Primary Cells and Cell Lines. *Acta Biomater.* **2010**, *6*, 1834–1842.

34. Lamaze, C.; Fujimoto, L. M.; Yin, H. L.; Schmid, S. L. The Actin Cytoskeleton Is Required for Receptor-Mediated Endocytosis in Mammalian Cells. *J. Biol. Chem.* **1997**, *272*, 20332–20335.

35. Zhang, H. Y.; Ji, Z. X.; Xia, T.; Meng, H.; Low-Kam, C.; Liu, R.; Pokhrel, S.; Lin, S. J.; Wang, X.; Liao, Y. P.; *et al.* Use of Metal Oxide Nanoparticle Band Gap to Develop a Predictive Paradigm for Oxidative Stress and Acute Pulmonary Inflammation. *ACS Nano* **2012**, *6*, 4349–4368.

36. Zhang, H. Y.; Dunphy, D. R.; Jiang, X. M.; Meng, H.; Sun, B. B.; Tarn, D.; Xue, M.; Wang, X.; Lin, S. J.; Ji, Z. X.; *et al.* Processing Pathway Dependence of Amorphous Silica Nanoparticle Toxicity: Colloidal Vs Pyrolytic. *J. Am. Chem. Soc.* **2012**, *134*, 15790–15804.

37. Castranova, V.; Schulte, P. A.; Zumwalde, R. D. Occupational Nanosafety Considerations for Carbon Nanotubes and Carbon Nanofibers. *Acc. Chem. Res.* **2013**, *46*, 642–649.

38. Koivisto, A. J.; Lyyranen, J.; Auvinen, A.; Vanhala, E.; Hameri, K.; Tuomi, T.; Jokiniemi, J. Industrial Worker Exposure to Airborne Particles During the Packing of Pigment and Nanoscale Titanium Dioxide. *Inhalation Toxicol.* **2012**, *24*, 839–849.

39. Yoon, H. K.; Moon, H. S.; Park, S. H.; Song, J. S.; Lim, Y.; Kohyama, N. Dendriform Pulmonary Ossification in Patient with Rare Earth Pneumoconiosis. *Thorax* **2005**, *60*, 701–703.

40. Waring, P. M.; Watling, R. J. Rare-Earth Deposits in a Deceased Movie Projectionist—A New Case of Rare-Earth Pneumoconiosis. *Med. J. Aust.* **1990**, *153*, 726–730.

41. Sulotto, F.; Romano, C.; Berra, A.; Botta, G. C.; Rubino, G. F.; Sabbioni, E.; Pietra, R. Rare-Earth Pneumoconiosis—A New Case. *Am. J. Ind. Med.* **1986**, *9*, 567–575.